ACS APPLIED ENERGY MATERIALS

www.acsaem.org
Article

Optimizing Discharge Rate for Li Metal Stability in Rechargeable Li|NMC Batteries under Lean Electrolyte Condition

Arghya Dutta,* Emiko Mizuki, Yuka Tomori, and Shoichi Matsuda*

Cite This: ACS Appl. Energy Mater. 2024, 7, 3824−3830
Read Online

ABSTRACT: Recent studies have highlighted the impressive performance of lithium metal batteries (LMBs), showcasing cell-level energy densities surpassing 350 Wh kg^{-1}. However, the intricate mechanisms leading to cell degradation in these batteries remain elusive, impeding their widespread utilization as energy storage devices. Specifically, the influence of the discharge rate on the deterioration of lithium metal electrodes remains poorly understood. In this study, pouch-type Li|NMC811 cells were fabricated employing a lean electrolyte, and a comprehensive exploration was conducted into the effects of the discharge rate on the battery performance. Intriguingly, our findings illustrate a positive correlation between the increase in discharge rate within the range of 0.4−1.6 mA cm^{-2} and an improvement in the cycle life of LMBs. In-depth analyses indicate that increasing the discharge current density to 1.6 mA cm^{-2} effectively suppresses irreversible volume expansion in lithium metal electrodes. Consequently, this suppression in volume expansion is identified as a significant factor contributing to the enhanced cycle life at increased discharge rates. Conversely, when the discharge rate surpasses 1.6 mA cm^{-2}, a detrimental impact on the cycle life is observed due to kinetic limitations experienced by the NMC electrode. These findings elucidate the operational principles governing LMBs, offering insights into achieving both high-power density and extended cycle life.

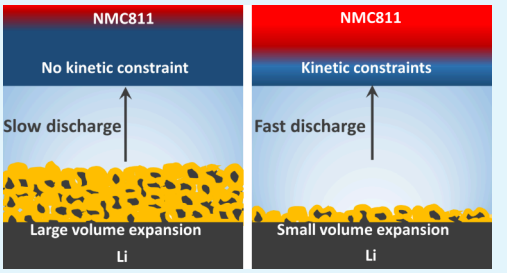

KEYWORDS: *lithium metal battery, high-capacity battery, failure analysis, discharge rate, battery diagnosis*

INTRODUCTION

Lithium metal batteries (LMBs) are a promising next-generation energy storage technology due to their high energy density.[1] However, their practical implementation is hindered by critical challenges, such as inefficient lithium (Li) plating/stripping, low Coulombic efficiency (CE), short cycle life, and dendrite formation.[2,3] Recent research efforts focusing on electrolyte optimization, particularly highly concentrated electrolytes, have shown significant progress in promoting stable, nondendritic Li deposition/dissolution, leading to improved CE, cycle life, and safety.[4−13] As a result, superior performance of LMBs with cell-level energy density higher than 350 Wh kg^{-1} with stable operation over 200 cycles could be achieved.[14] Despite these achievements, the intricate degradation mechanism of Li metal electrodes, distinct from that of conventional graphite electrodes, remains obscure, limiting their widespread practical application. Particularly, understanding the impact of charge/discharge rates on the degradation of Li metal is vital given the varied rates required in many practical applications. In this regard, several studies have extensively probed the influence of charging rates on LMB performance, revealing an inverse correlation with stability and cycle life.[15,16] High charging rates lead to issues such as uneven Li plating, dendritic morphologies, volume expansion, and cell short-circuits due to long-range diffusion limitations and inhomogeneous current density distribution. In contrast, the effect of the discharging rate on the performance of LMBs remains unclear. Recent studies have observed that LMBs exhibit enhanced cycle life due to the improved stability of the Li electrode when discharged at relatively higher rates than the charging rates.[17,18] However, these studies employed a maximum discharge current density of 3 mA cm^{-2} (0.5−1 C depending on the positive electrode loading), leaving the potential effects of higher rates unexplored. As a result, the true impact of a wide range of discharge current densities on the stability of the Li electrode and the overall performance of LMBs remains elusive. Thus, to develop LMBs capable of delivering high-power discharge, a comprehensive understanding of the effects of high discharge rates on the stability of high-energy LMBs is crucial. This necessitates a systematic investigation of the Li electrode cycled under a broad range of discharge current densities coupled with an analysis of the underlying kinetic factors.

Based on these research backgrounds, in this study, we investigated the impact of discharging rates ranging from 0.4

Received: January 23, 2024
Revised: March 20, 2024
Accepted: April 8, 2024
Published: April 19, 2024

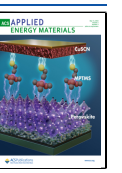

mA cm^{-2} up to a very high value of 8.0 mA cm^{-2} on the degradation of the Li metal electrode and the kinetic limitations in pouch-type LilNMC811 cells with a lean electrolyte. To ensure a comparable assessment, we uniformly maintained the charge current density and the cycled capacity at 0.4 mA cm^{-2} and 4 mAh cm^{-2}, respectively, while the discharge current density was varied across all cells. Notably, our findings indicate a favorable impact of increased discharge rates within the 0.4−1.6 mA cm^{-2} range on improving the cycle life of LMBs. Comprehensive analytical assessments indicate that the effective suppression of irreversible volume expansion in Li metal electrodes under high discharge rates can be attributed to one of the major reasons behind this noteworthy improvement in cycle life. In contrast, discharge rates exceeding 1.6 mA cm^{-2} exhibit a detrimental effect on cycle life, attributed to kinetic limitations observed at the NMC electrode. These revelations significantly contribute to comprehending the interplay between discharge current density and the behavior of pouch-type LilNMC811 cells featuring lean electrolytes, bearing profound implications for the practical advancement of high-energy-density and high-power LMBs.

EXPERIMENTAL METHODS

Electrolyte. A solution of lithium bis(fluorosulfonyl)imide (LiFSI) in 1,2-dimethoxyethane (DME) was prepared with a Li$^+$ concentration of 4 M. Both LiFSI and DME were obtained from Kishida Chemical Co., Ltd., with purity >99.0 and >99.5%, respectively.

Positive Electrode. A mixture comprising lithium nickel manganese cobalt oxide ($LiNi_{0.8}Mn_{0.1}Co_{0.1}O_2$ or NMC811) active material (94 wt %), acetylene black (Denka Black HS100; obtained from DENKA Co.; 3 wt %), and polyvinylidene fluoride (PVDF; sourced from KUREHA Co.; 3 wt %) binder dissolved in *N*-methyl-1,2-pyrrolidone (NMP; super-dehydrated; obtained from FUJIFILM Wako Pure Chemical Co.) was spread onto an aluminum (Al) current collector (with a thickness of 20 μm). The NMP solvent was evaporated by heating at 230 °C in a nitrogen atmosphere for 30 min, resulting in the production of electrode sheets with a loading amount of the active materials of approximately 30 mg cm^{-2}.

Negative Electrode. The negative electrode employed in the study consisted of a 50 μm thick Li on a 10 μm thick copper (Cu) current collector (Honjo Metal Co., Ltd.).

Cell Fabrication. A laminated pouch cell was assembled with a positive electrode (40 mm × 30 mm), a separator (Teijin, 46 mm × 36 mm), and a negative electrode (42 mm × 32 mm) stacked inside. Three sides of the pouch were sealed, and 120 μL of electrolyte (10 μL cm^{-2}, approximately 2 g Ah^{-1} considering the NMC811 loading) was injected before the remaining side was sealed under vacuum. All cells were assembled inside a dry room with the dew point below −50 °C, and electrolyte injection was performed in a fume hood with the dew point below −85 °C.

Charge/Discharge Protocol. The cells were charged and discharged at 25 °C using a Hokuto Denko HJ1001SD8 battery cycler. All cells were cycled at a constant charge current density of 0.4 mA cm^{-2} with a limited capacity of 4.0 mAh cm^{-2} in the voltage range 2−4.2 V versus Li/Li$^+$. Five different discharge current densities were applied: 0.4, 0.8, 1.6, 4.0, and 8.0 mA cm^{-2}. For the constant current constant voltage (CCCV) discharge protocols, the cells underwent discharge at various constant current densities of up to 2.0 V versus Li/Li$^+$. Subsequently, a constant voltage step was implemented at 2.0 V versus Li/Li$^+$ until the current value fell below 0.04 mA cm^{-2}.

Electrochemical Impedance Spectroscopy (EIS). EIS measurements were performed on the cells using a Biologic VMP3 potentiostat/galvanostat in the frequency range of 100 kHz−10 mHz with a potential amplitude of 10 mV. The Ohmic resistance of the cells was determined from the intersection of the Nyquist plot with the real axis in the high-frequency limit. The interphasial impedance corresponding to the negative electrode was determined from the diameter of the semicircle in the high-to-midfrequency range of the Nyquist plots.

X-ray CT Measurement. X-ray computed tomography (XCT) analysis of pouch cells was performed using an Xradia 520 Versa instrument (ZEISS, Germany) with a source voltage of 140 kV and power of 10 W. Following a certain number of charge/discharge cycles, cells were mounted on the sample holder and rotated 360° for 4501 scans, each with an exposure time of 10 s. The XCT images had a pixel resolution of 3.385 μm.

RESULTS AND DISCUSSION

In our present research, we fabricated LMBs featuring a high-nickel-content lithium nickel manganese cobalt oxide ($LiNi_{0.8}Mn_{0.1}Co_{0.1}O_2$ or NMC811) positive electrode, a thin Li metal negative electrode (50 μm), and a lean electrolyte condition (10 μL cm^{-2} or around 2 g Ah^{-1}). The electrolyte used was 4 M lithium bis(fluorosulfonyl)imide (LiFSI) in dimethoxy ethane (DME). A schematic representation of the pouch cell is shown in Figure 1a. We first examined the

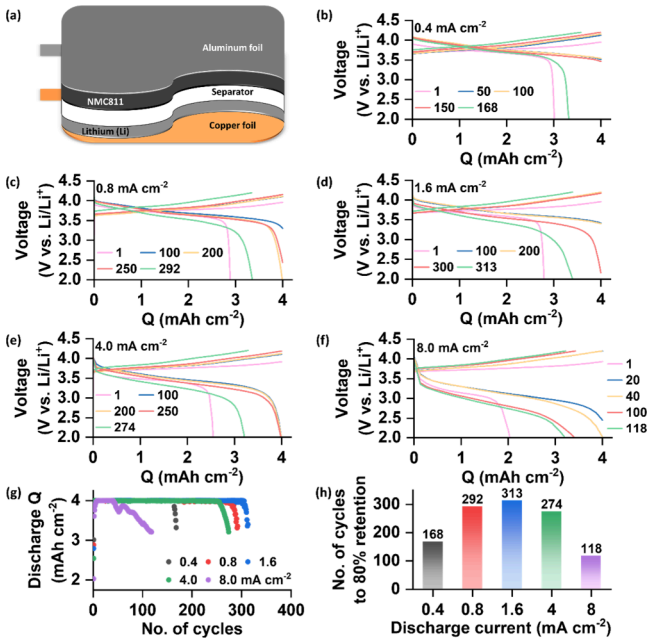

Figure 1. (a) Schematic representation of the pouch cell used in this study. (b−f) Galvanostatic charge/discharge curves of selected cycles for the cells charged at 0.4 mA cm^{-2} and discharged at 0.4, 0.8, 1.6, 4.0, and 8.0 mA cm^{-2}, respectively, with the fixed capacity set at 4 mAh cm^{-2}. (g) Discharge capacity (Q) vs cycle number plots for the same cells as in (b−f). (h) Bar diagram showing the number of cycles before the discharge capacity drops below 80% of the initially set capacity of 4 mAh cm^{-2}.

influence of the discharging rate on the LMB cycle performance. All the fabricated LMB cells were charged at a fixed current density (0.4 mA cm^{-2}) and subsequently discharged at varying current densities: 0.4, 0.8, 1.6, 4.0, and 8.0 mA cm^{-2}. During these charge/discharge processes, we limited the cycle capacity to 4 mAh cm^{-2} to avoid any undesired overcharging phenomenon. Notably, a fixed charge current density and limited cycle capacity enable delineating the influence of discharge current density on the cell performance.

The galvanostatic charge/discharge curves for selected cycles are depicted in Figure 1b−f, where the highest cycle number

https://doi.org/10.1021/acsaem.4c00180
ACS Appl. Energy Mater. 2024, 7, 3824−3830

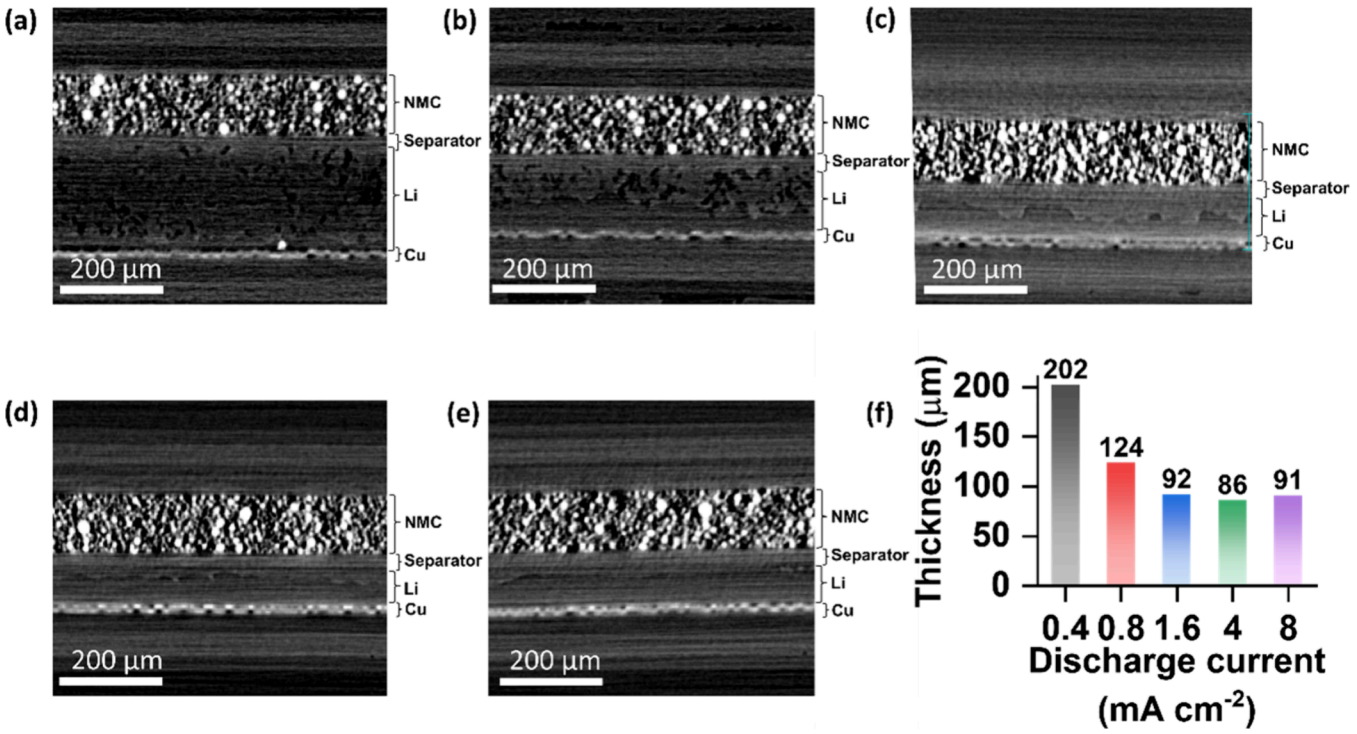

Figure 2. (a–e) Cross-section XCT images of the pouch cells after 50 cycles at a charge current density of 0.4 mA cm^{-2} and a discharge current density of 0.4, 0.8, 1.6, 4.0, and 8.0 mA cm^{-2}, respectively. (f) Bar diagram showing the thickness of the Li metal electrode after 50 cycles.

displayed signifies the cycle at which the capacity (Q) of the cell drops below 3.2 mAh cm^{-2}, which is 80% of its set capacity. The results reveal an intriguing pattern of capacity retention, which becomes even more evident in Figure 1g,h. With the increase in the discharge current density from 0.4 to 0.8 and 1.6 mA cm^{-2}, cycling stability demonstrates an enhancement, reaching 168, 292, and 313 cycles, respectively. However, further increasing the discharge current density to 4.0 and 8.0 mA cm^{-2} diminishes the cycling stability to 274 and 118 cycles, respectively. The voltage–time curves depicted in Figure S1a–e indicate that cell failure cannot be ascribed to a short circuit in any of these cases. Instead, a distinct rise in voltage polarization becomes evident from Figures S2 and S3 as the cycles progress across all instances. This voltage polarization, when prematurely reaching the cutoff potential, results in a lower capacity compared to the predetermined value. Therefore, to elucidate the correlation between discharge rate and cycle life, it is crucial to meticulously examine the evolution of discharge-voltage polarization and its dependence on discharge rates throughout the cycles.

Since Li electrode degradation is the most significant reason for cell failure in LMBs, to attain an intricate insight into the structural changes of Li electrodes, we performed XCT analysis on the pouch cells after 50 cycles. One remarkable advantage of utilizing XCT lies in its nondestructive characteristic, enabling analysis without causing damage to either the cell or electrodes during measurement.[17,19] Notably, XCT analysis furnishes valuable information regarding the physical transformation of Li metal electrodes and facilitates the estimation of changes in their thickness. The cross-sectional XCT images of the pouch cells after 50 cycles are depicted in Figure 2a–e. Noteworthy observations emerge from Figure 2a, revealing a substantial expansion of the Li electrode with notable porosity in the cycled portion when discharged at 0.4 mA cm^{-2}. On the other hand, increasing the discharge current density to 0.8 and 1.6 mA cm^{-2} effectively suppresses the thickness growth of the Li electrode, as evident in Figure 2b,c, respectively. However, the findings presented in Figure 2d,e demonstrate that a further increase in discharge current density to 4.0 and 8.0 mA cm^{-2} does not provide additional advantageous effects in suppressing the expansion of the Li electrode. A quantitative comparison of Li electrode swelling after 50 cycles, exhibited in Figure 2f, underscores the extent of these changes. Cycling at 0.4 mA cm^{-2} leads to an expansion of the Li electrode thickness from an initial 50 μm to an astonishing 202 μm. Increasing the discharge current density to 0.8 and 1.6 mA cm^{-2} limits this thickness to 124 and 92 μm, respectively. Interestingly, when discharge current densities of 4.0 and 8.0 mA cm^{-2} are implemented, the Li electrode thickness measures to be 86 and 91 μm, respectively. These results clearly reveal that the increase in discharge rate is beneficial for suppressing the undesired irreversible volume expansion of the Li metal electrodes.

We also conducted electrochemical impedance spectroscopic analysis of the cells to acquire quantitative information about the internal resistance. Details of the EIS analyses are provided in Experimental Methods, and the Nyquist plots are presented in Figure 3a–e. Figure 3f offers insights into the changes in Ohmic resistance (R_{Ohmic}), representing the contact and electrolyte resistances of the cells. Notably, all cells discharged at different current densities exhibited a gradual increase in R_{Ohmic} throughout the cycling. However, intriguingly, the cells discharged at a rate of 0.4 mA cm^{-2} showed a rapid increase in R_{Ohmic} beyond 70 cycles, reaching over 3 Ω after 100 cycles. In contrast, the cells with a discharge rate of 0.8 mA cm^{-2} or higher exhibited a limited increase in R_{Ohmic}. In Figure 3g, the changes in interphasial resistance (R_{Int}) over the cycles are also depicted, revealing an increasing trend of R_{Int} as

https://doi.org/10.1021/acsaem.4c00180
ACS Appl. Energy Mater. 2024, 7, 3824–3830

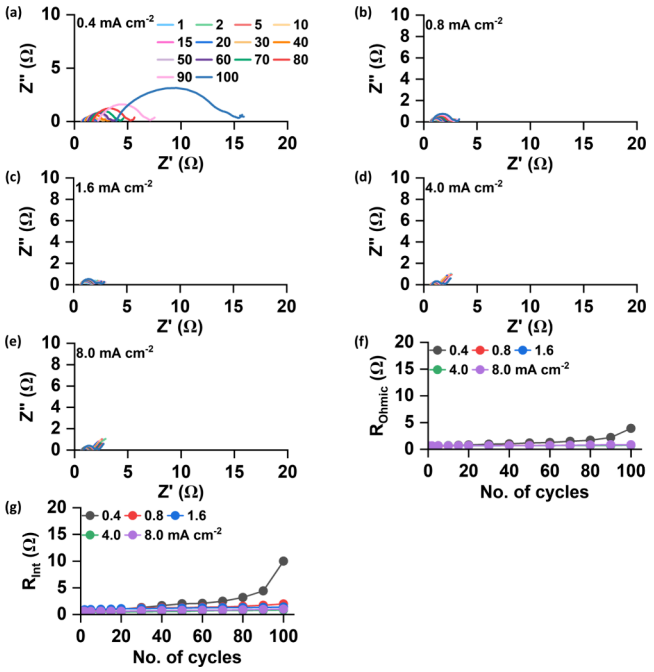

Figure 3. (a–e) Nyquist plots after selected cycles for the cells charged at 0.4 mA cm^{-2} and discharged at 0.4, 0.8, 1.6, 4.0, and 8.0 mA cm^{-2}, respectively. (f) Changes in Ohmic resistance (R_{Ohmic}) and (g) interphasial resistance (R_{Int}) of the cells over the cycles.

the cycles progress for all cells. Even for R_{Int}, trends similar to those of R_{Ohmic} are observed. The cell discharged at a rate of 0.4 mA cm^{-2} exhibited a significant increase in R_{Int} as the cycles progressed, and the value of R_{Int} exceeded 10 Ω on the 100th cycle. In sharp contrast, in the cells with a discharge rate higher than 0.4 mA cm^{-2}, the value of R_{Int} remained less than 2 Ω after 100 cycles. These results clearly highlight the substantial impact of the discharge rate on the increase in internal resistance.

Based on the results of XCT and impedance analyses, let us summarize the impact of the discharge rate on the performance of the LilNMC811 cell. XCT analysis reveals that increasing the discharge rate in the range of 0.4–1.6 mA cm^{-2} significantly suppresses the volume expansion of the lithium metal electrode. Under high-rate discharge conditions, the stripping of Li particles primarily occurs at the tips and corners of the deposit, where equipotential lines are concentrated. This high-rate Li stripping reduces inhomogeneity and suppresses the formation of dead Li. Additionally, this reduced inhomogeneity decreases the surface area of Li exposed to the electrolyte, leading to a decrease in the level of accumulation of SEI compounds. Consequently, the volume expansion of the electrode is constrained under high-rate discharge conditions. Figure 4 schematically shows a proposed mechanism of Li dissolution under high and low rates of discharge. According to this mechanism, the suppressed volume expansion indicates less depletion of active Li and reduced accumulation of SEI products, collectively benefiting cell performance. Due to the relatively low electrolyte content (approximately 2 g Ah^{-1}) in the cells, the entrapped electrolyte within the expanded porous electrode results in an electrolyte shortage. This electrolyte deficiency, coupled with the growth of the insulating SEI layer, exacerbates impedance growth within the cell at low discharge rates. Consequently, increasing the current density within the range of 0.4–1.6 mA cm^{-2} has a beneficial effect on enhancing the cycle life of the cell. While impedance growth is also expected on the NMC811 electrode side during cycling, the correlation between discharge rate-

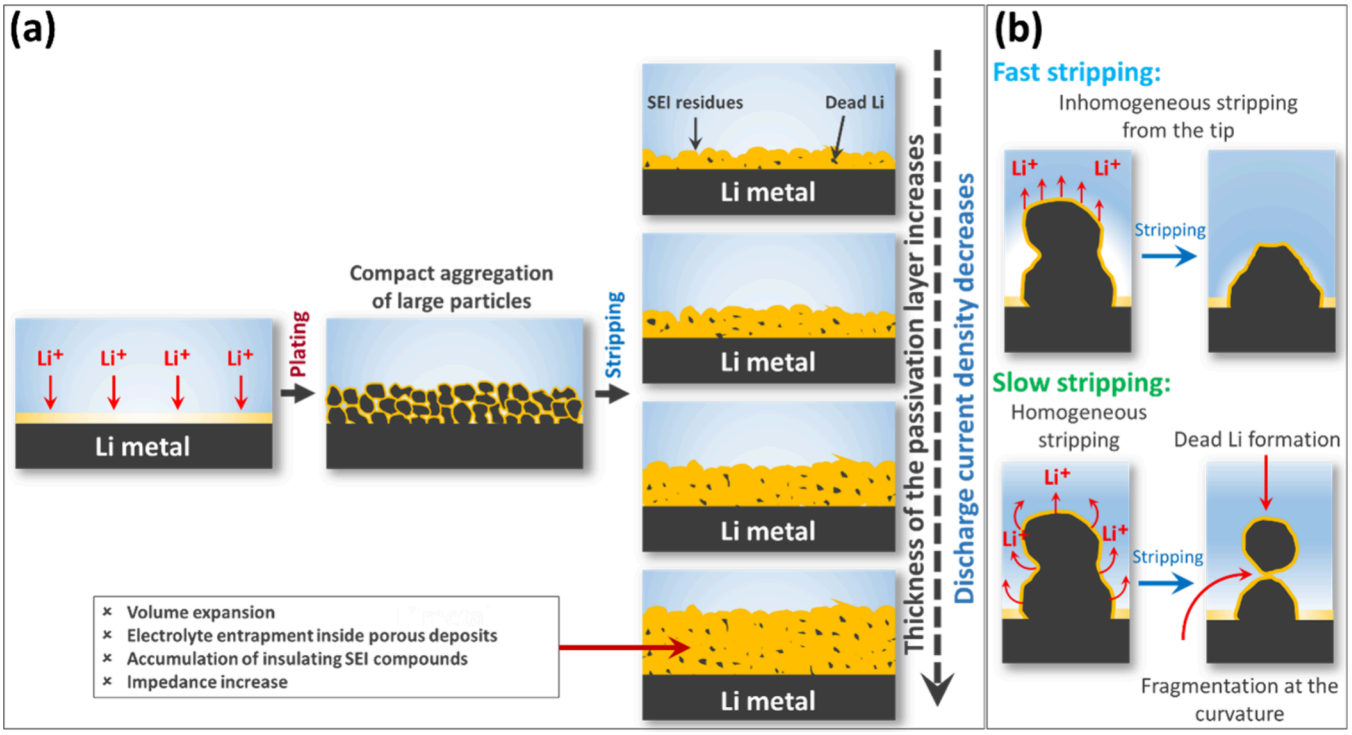

Figure 4. (a) Schematic representation of the Li plating–stripping cycles at different rates of discharge. (b) Explanation of Li-stripping processes at fast and slow rates.

https://doi.org/10.1021/acsaem.4c00180
ACS Appl. Energy Mater. 2024, 7, 3824–3830

dependent Li electrode expansion and increasing impedance is evident.

Next, we turned our attention to investigating the reason for the decreasing cycle life of Li|NMC811 cells at discharge current densities above 1.6 mA cm^{-2}. Apart from the factors originating from the Li negative electrode, various detrimental mechanisms from the NMC811 positive electrode side also contribute collectively to the termination of cell life.[20−25] One significant aspect of this electrode degradation is the parasitic reaction of the electrolyte on the surface of NMC811 under highly delithiated conditions (high state of charge).[23−25] This environment promotes chemical reactions between Ni^{4+} ions and the electrolyte, leading to the dissolution of transition metals and the formation of an electrically insulating interphasial layer. Other degradation processes experienced by NMC811 include increased Li/Ni mixing, structural transformations that give rise to the formation of spinel and rock-salt structures on the surface, and particle cracking, among others.[20−22] These degradation processes hinder Li^+ diffusion transport between the bulk lattice and electrolyte and contribute to irreversible capacity loss. Since all the cells in our experiments were charged uniformly at the same current density of 0.4 mA cm^{-2} to a consistent cutoff potential of 4.2 V versus Li/Li^+ for a fixed capacity of 4.0 mAh cm^{-2}, it can be assumed that the extent of electrolyte decomposition and its subsequent impact on the positive electrode during the charging process is relatively similar across all cells.

Based on the above considerations, we performed the CCCV discharge test to deconvolute the reversible and irreversible capacity losses originating from the NMC811 positive electrode. During the constant voltage (CV) discharge process at 2.0 V, the capacity loss due to kinetic limitations during variable rate constant current discharge can be recovered.[26] The corresponding charge−discharge voltage profiles for the first cycle are depicted in Figure 5a. At the end of galvanostatic discharge (CC step), all cells exhibited CE values significantly below 100%. Notably, as the discharge current density increased, the first-cycle CE gradually diminished, indicating greater capacity loss at higher rates.

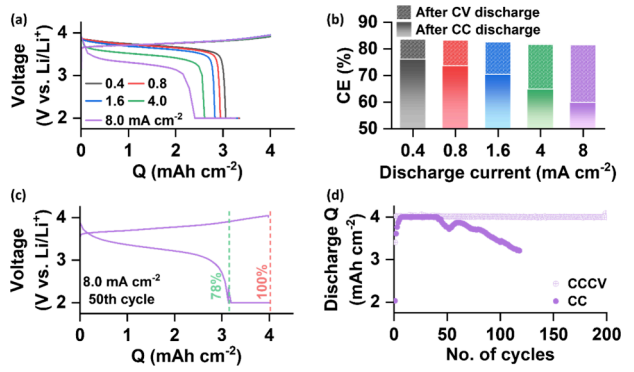

Figure 5. (a) Charge/discharge voltage profiles of the first cycle for the cells charged at a constant current density of 0.4 mA cm^{-2} and discharged under a CCCV protocol with varied discharge current densities, followed by a constant voltage hold at 2.0 V. (b) Bar diagram showing the first cycle CE of the cells before and after the employment of the CV step. (c) Charge/discharge voltage profile of the 50th cycle for the cell discharged at a current density of 8.0 mA cm^{-2} under the CCCV protocol. (d) Comparison of discharge capacity (Q) retention between cells discharged under CC and CCCV protocols at a current density of 8.0 mA cm^{-2}.

For example, as illustrated in Figure 5b, the cell discharged at 0.4 mA cm^{-2} demonstrated a first-cycle CE of 76%. In contrast, a mere 60% CE was attained when the cell underwent a discharge at 8.0 mA cm^{-2}. Remarkably, after the CV discharge, all cells recovered a certain amount of capacity, with cells discharged at higher discharge current densities showing more substantial recovery. As a result of the CV discharge, all cells exhibited comparable first-cycle CE values within the range of 81−84%. These results provide clear insights into the significant influence of kinetic limitations (Li^+ diffusion in both electrolyte and NMC811) on capacity loss during high-rate discharge.

Observing a significant capacity loss in the first cycle due to kinetic constraints, we also performed a similar CCCV discharge protocol for long cycles in the case of 8.0 mA cm^{-2} discharge current density to clarify the origin of capacity fading during cycling at high discharge rates. Figure 5c illustrates the voltage profile during the 50th cycle under the CCCV discharge protocol at a rate of 8.0 mA cm^{-2}. The findings reveal that at the end of the CC step the discharge capacity reached 78% of the set value of 4 mAh cm^{-2}. However, when the CV step was applied, 100% of the capacity was recovered. Additionally, in Figure 5d, we compared the capacity retention trends between CC and CCCV discharges at 8.0 mA cm^{-2}. While the capacity under CC discharge exhibited fluctuations above 50 cycles and dropped below 80% of the set capacity within 118 cycles, the CCCV discharge retained 100% capacity for at least 200 cycles. Thus, it becomes evident that in the case of CC discharge at 8.0 mA cm^{-2}, the capacity degradation primarily occurred due to kinetic limitations within the cell.

CONCLUSIONS

In summary, we conducted an in-depth analysis to investigate the effects of discharge current densities, reaching an ultrahigh value of 8.0 mA cm^{-2}, in Li|NMC811 pouch cells utilizing a lean electrolyte. Employing a nondestructive ex situ XCT technique, we delved into the evolution of Li electrodes, which experience volume expansion during cycling, attributed to the accumulation of both electrically isolated dead Li and SEI compounds. Our XCT findings provide compelling evidence that increasing the discharge current density up to a certain threshold of 1.6 mA cm^{-2} effectively curtails the volume expansion of the Li electrode. However, any further rise in discharge current density does not yield additional benefits, nor do we observe any detrimental consequences. The capacity retention and cycling stability trends of the cells discharged at varying rates reveal intriguing observations. Increasing the discharge current density from 0.4 to 1.6 mA cm^{-2} enhances cycling stability, directly aligning with the suppressed volume expansion of the Li electrode at higher discharge rates. Although the gradual deterioration of the NMC811 electrode and impedance growth at its interface may also affect capacity fading and require further analysis, the correlation between the cycle life and discharge rate-dependent evolution of the Li electrode up to a current density of 1.6 mA cm^{-2} is evident. These observations unequivocally demonstrate the beneficial effect of increasing the discharge current density up to 1.6 mA cm^{-2} for a higher stability of the Li electrode, resulting in an improved cycle life. Conversely, further increasing the rate to 4.0 and 8.0 mA cm^{-2} exhibits a declining trend in capacity retention. While the negative electrode is not adversely affected by a high discharge rate, our kinetic analysis has established

https://doi.org/10.1021/acsaem.4c00180
ACS Appl. Energy Mater. 2024, 7, 3824−3830

that a high discharge current density triggers capacity loss due to inefficient Li kinetics within the cell. Kinetic limitations at high discharge rates increase the discharge overpotential. Consequently, this leads to premature reaching of cutoff conditions with higher discharge overpotential and lower capacity, ultimately resulting in a shorter cycle life. Therefore, the combined effects of the stability of the Li electrode and kinetic constraints have identified an intermediate discharge rate, offering a superior cycle life. The findings presented contribute to a deeper understanding of Li metal electrode stabilization and kinetic constraints in a high-energy-density LMB under ultrahigh discharge current rates. These unprecedented insights hold significant implications for advancing high-power and high-energy LMBs for practical applications.

■ ASSOCIATED CONTENT

Supporting Information

The Supporting Information is available free of charge at https://pubs.acs.org/doi/10.1021/acsaem.4c00180.

Voltage−time curves of the cells discharged at different current rates, average discharge, and charge voltage versus cycle number plots (PDF)

■ AUTHOR INFORMATION

Corresponding Authors

Arghya Dutta − *Center for Green Research on Energy and Environmental Materials, National Institute for Materials Science, Tsukuba 305-0044 Ibaraki, Japan;* orcid.org/0000-0002-3769-7820; Email: DUTTA.Arghya@nims.go.jp

Shoichi Matsuda − *Center for Green Research on Energy and Environmental Materials, NIMS-SoftBank Advanced Technologies Development Center, and Center for Advanced Battery Collaboration, Center for Green Research on Energy and Environmental Materials, National Institute for Materials Science, Tsukuba 305-0044 Ibaraki, Japan;* orcid.org/0000-0002-0640-3404; Email: MATSUDA.Shoichi@nims.go.jp

Authors

Emiko Mizuki − *Center for Green Research on Energy and Environmental Materials, National Institute for Materials Science, Tsukuba 305-0044 Ibaraki, Japan*

Yuka Tomori − *Center for Green Research on Energy and Environmental Materials, National Institute for Materials Science, Tsukuba 305-0044 Ibaraki, Japan*

Complete contact information is available at: https://pubs.acs.org/10.1021/acsaem.4c00180

Funding

JST COI-NEXT Grant Number JPMJPF2016.

Notes

The authors declare no competing financial interest.

■ ACKNOWLEDGMENTS

The present work was partially supported by JST COI-NEXT Grant Number JPMJPF2016. This work also received support from the National Institute for Materials Science (NIMS) Battery Research Platform.

■ REFERENCES

(1) Lin, D.; Liu, Y.; Cui, Y. Reviving the Lithium Metal Anode for High-Energy Batteries. *Nat. Nanotechnol.* **2017**, *12*, 194−206.

(2) Horstmann, B.; Shi, J.; Amine, R.; Werres, M.; He, X.; Jia, H.; Hausen, F.; Cekic-Laskovic, I.; Wiemers-Meyer, S.; Lopez, J.; Galvez-Aranda, D.; Baakes, F.; Bresser, D.; Su, C.-C.; Xu, Y.; Xu, W.; Jakes, P.; Eichel, R.-A.; Figgemeier, E.; Krewer, U.; Seminario, J. M.; Balbuena, P. B.; Wang, C.; Passerini, S.; Shao-Horn, Y.; Winter, M.; Amine, K.; Kostecki, R.; Latz, A. Strategies towards Enabling Lithium Metal in Batteries: Interphases and Electrodes. *Energy Environ. Sci.* **2021**, *14*, 5289−5314.

(3) Hobold, G. M.; Lopez, J.; Guo, R.; Minafra, N.; Banerjee, A.; Shirley Meng, Y.; Shao-Horn, Y.; Gallant, B. M. Moving beyond 99.9% Coulombic Efficiency for Lithium Anodes in Liquid Electrolytes. *Nat. Energy* **2021**, *6*, 951−960.

(4) Qian, J.; Henderson, W. A.; Xu, W.; Bhattacharya, P.; Engelhard, M.; Borodin, O.; Zhang, J.-G. High Rate and Stable Cycling of Lithium Metal Anode. *Nat. Commun.* **2015**, *6*, 6362.

(5) Chen, S.; Zheng, J.; Mei, D.; Han, K. S.; Engelhard, M. H.; Zhao, W.; Xu, W.; Liu, J.; Zhang, J.-G. High-Voltage Lithium-Metal Batteries Enabled by Localized High-Concentration Electrolytes. *Adv. Mater.* **2018**, *30*, No. 1706102.

(6) Jiao, S.; Ren, X.; Cao, R.; Engelhard, M. H.; Liu, Y.; Hu, D.; Mei, D.; Zheng, J.; Zhao, W.; Li, Q.; Liu, N.; Adams, B. D.; Ma, C.; Liu, J.; Zhang, J.-G.; Xu, W. Stable Cycling of High-Voltage Lithium Metal Batteries in Ether Electrolytes. *Nat. Energy* **2018**, *3*, 739−746.

(7) Markevich, E.; Salitra, G.; Chesneau, F.; Schmidt, M.; Aurbach, D. Very Stable Lithium Metal Stripping−Plating at a High Rate and High Areal Capacity in Fluoroethylene Carbonate-Based Organic Electrolyte Solution. *ACS Energy Lett.* **2017**, *2*, 1321−1326.

(8) Ren, X.; Zou, L.; Jiao, S.; Mei, D.; Engelhard, M. H.; Li, Q.; Lee, H.; Niu, C.; Adams, B. D.; Wang, C.; Liu, J.; Zhang, J.-G.; Xu, W. High-Concentration Ether Electrolytes for Stable High-Voltage Lithium Metal Batteries. *ACS Energy Lett.* **2019**, *4*, 896−902.

(9) Chen, J.; Zhang, H.; Fang, M.; Ke, C.; Liu, S.; Wang, J. Design of Localized High-Concentration Electrolytes via Donor Number. *ACS Energy Lett.* **2023**, *8*, 1723−1734.

(10) Ruan, D.; Tan, L.; Chen, S.; Fan, J.; Nian, Q.; Chen, L.; Wang, Z.; Ren, X. Solvent versus Anion Chemistry: Unveiling the Structure-Dependent Reactivity in Tailoring Electrochemical Interphases for Lithium-Metal Batteries. *J. Am. Chem. Soc. Au* **2023**, *3*, 953−963.

(11) Chen, Y.; Li, M.; Liu, Y.; Jie, Y.; Li, W.; Huang, F.; Li, X.; He, Z.; Ren, X.; Chen, Y.; Meng, X.; Cheng, T.; Gu, M.; Jiao, S.; Cao, R. Origin of Dendrite-Free Lithium Deposition in Concentrated Electrolytes. *Nat. Commun.* **2023**, *14*, 2655.

(12) Zhao, Y.; Zhou, T.; Mensi, M.; Choi, J. W.; Coskun, A. Electrolyte Engineering via Ether Solvent Fluorination for Developing Stable Non-Aqueous Lithium Metal Batteries. *Nat. Commun.* **2023**, *14*, 299.

(13) Zhao, Y.; Zhou, T.; Ashirov, T.; Kazzi, M. El; Cancellieri, C.; Jeurgens, L. P. H.; Choi, J. W.; Coskun, A. Fluorinated Ether Electrolyte with Controlled Solvation Structure for High Voltage Lithium Metal Batteries. *Nat. Commun.* **2022**, *13*, 2575.

(14) Niu, C.; Lee, H.; Chen, S.; Li, Q.; Du, J.; Xu, W.; Zhang, J.-G.; Whittingham, M. S.; Xiao, J.; Liu, J. High-Energy Lithium Metal Pouch Cells with Limited Anode Swelling and Long Stable Cycles. *Nat. Energy* **2019**, *4*, 551−559.

(15) Bai, P.; Li, J.; Brushett, F. R.; Bazant, M. Z. Transition of Lithium Growth Mechanisms in Liquid Electrolytes. *Energy Environ. Sci.* **2016**, *9*, 3221−3229.

(16) Lu, D.; Shao, Y.; Lozano, T.; Bennett, W. D.; Graff, G. L.; Polzin, B.; Zhang, J.; Engelhard, M. H.; Saenz, N. T.; Henderson, W. A.; Bhattacharya, P.; Liu, J.; Xiao, J. Failure Mechanism for Fast-Charged Lithium Metal Batteries with Liquid Electrolytes. *Adv. Energy Mater.* **2015**, *5*, No. 1400993.

(17) Dutta, A.; Mizuki, E.; Matsuda, S. High-Rate Discharge Minimizes Volume Expansion of Lithium Metal Electrodes under Lean Electrolyte and High Areal Capacity Conditions. *Batteries Supercaps* **2023**, *6*, No. e202300309.

(18) Louli, A. J.; Coon, M.; Genovese, M.; de Gooyer, J.; Eldesoky, A.; Dahn, J. R. Optimizing Cycling Conditions for Anode-Free Lithium Metal Cells. *J. Electrochem. Soc.* **2021**, *168*, No. 020515.
(19) Tamate, R.; Matsuda, S. Asymmetric Volume Expansion of the Lithium Metal Electrode in Symmetric Lithium/Lithium Cells under Lean Electrolyte and High Areal Capacity Conditions. *ACS Appl. Energy Mater.* **2023**, *6*, 573−579.
(20) Märker, K.; Reeves, P. J.; Xu, C.; Griffith, K. J.; Grey, C. P. Evolution of Structure and Lithium Dynamics in $LiNi_{0.8}Mn_{0.1}Co_{0.1}O_2$ (NMC811) Cathodes during Electrochemical Cycling. *Chem. Mater.* **2019**, *31*, 2545−2554.
(21) Kondrakov, A. O.; Schmidt, A.; Xu, J.; Geßwein, H.; Mönig, R.; Hartmann, P.; Sommer, H.; Brezesinski, T.; Janek, J. Anisotropic Lattice Strain and Mechanical Degradation of High- and Low-Nickel NCM Cathode Materials for Li-Ion Batteries. *J. Phys. Chem. C* **2017**, *121*, 3286−3294.
(22) Streich, D.; Erk, C.; Guéguen, A.; Müller, P.; Chesneau, F.-F.; Berg, E. J. Operando Monitoring of Early Ni-Mediated Surface Reconstruction in Layered Lithiated Ni−Co−Mn Oxides. *J. Phys. Chem. C* **2017**, *121*, 13481−13486.
(23) Langdon, J.; Sim, R.; Manthiram, A. Gas Generation in Lithium Cells with High-Nickel Cathodes and Localized High-Concentration Electrolytes. *ACS Energy Lett.* **2022**, *7*, 2634−2640.
(24) Ren, X.; Gao, P.; Zou, L.; Jiao, S.; Cao, X.; Zhang, X.; Jia, H.; Engelhard, M. H.; Matthews, B. E.; Wu, H.; Lee, H.; Niu, C.; Wang, C.; Arey, B. W.; Xiao, J.; Liu, J.; Zhang, J.-G.; Xu, W. Role of Inner Solvation Sheath within Salt−Solvent Complexes in Tailoring Electrode/Electrolyte Interphases for Lithium Metal Batteries. *Proc. Natl. Acad. Sci. U. S. A.* **2020**, *117*, 28603−28613.
(25) Jia, H.; Xu, Y.; Burton, S. D.; Gao, P.; Zhang, X.; Matthews, B. E.; Engelhard, M. H.; Zhong, L.; Bowden, M. E.; Xiao, B.; Han, K. S.; Wang, C.; Xu, W. Enabling Ether-Based Electrolytes for Long Cycle Life of Lithium-Ion Batteries at High Charge Voltage. *ACS Appl. Mater. Interfaces* **2020**, *12*, 54893−54903.
(26) Zhou, H.; Xin, F.; Pei, B.; Whittingham, M. S. What Limits the Capacity of Layered Oxide Cathodes in Lithium Batteries? *ACS Energy Lett.* **2019**, *4*, 1902−1906.

https://doi.org/10.1021/acsaem.4c00180
ACS Appl. Energy Mater. 2024, 7, 3824−3830